

Two problems on the flow of viscous sheets of molten glass

“Flows related to drawing of viscous sheets” problem presented by

Dr. John Abbott
Corning Incorporated
Advanced Modeling and Analysis group
Corning New York

Participants:

Sean Bohun	Ian Griffiths	Alexander Volfson
Chris Breward	Russ Howes	Tom Witeliski
Ivan Christov	Dave Martin	Haley Yapple
Linda Cummings	Javed Siddique	
Don Drew	David Sondak	

Summary Presentation given by Ian Griffiths (6/18/10)

Summary Report compiled by Sean Bohun, Chris Breward, Linda Cummings and Tom Witeliski

Abstract

The problem brought to the 2010 Mathematical Problems in Industry Workshop by Corning Incorporated involved a manufacturing process for the production of high-quality thin glass sheets for many commercial applications (large screen video displays for example). The process begins with hot molten glass flowing out of an apparatus (essentially an overflowing triangular trough) that helps distribute the material into uniform sheets of desired width and controlled thickness. The design of the apparatus is fundamentally based on exploiting fluid dynamics to control the process. The MPI Workshop studied the fluid dynamics of two distinct stages of the process during the MPI workshop. Formulation of sound mathematical models of the glass flow were the basis for numerical simulations and stability analysis that can provide important insight on improving the reliability of the sheet production process.

1 Introduction

The basic sheet glass production process considered by the workshop is illustrated schematically in Figs.1 through 4. A trough is filled with molten glass via an inlet, as shown in Fig.1 (the inlet is on the left in this figure). The exterior of the trough is a symmetric triangular wedge, while its interior is a sloped, more shallow, wedge (indicated by a dashed line in Fig.1). As the trough’s interior reservoir is filled, the molten glass overflows, and cascades down the two exterior walls of the trough. The two cascading sheets meet at the trough’s underside, coalesce, and form a single viscous sheet. This hanging sheet continues to fall under gravity, and also under external drawing forces that may be applied. As the sheet falls in this “extensional flow” regime it thins, and eventually is cooled and solidified downstream, at an appropriate final thickness. Clearly the whole production process relies on the system design generating the correct fluid dynamics. The desired outcome is a sheet of desired thickness and uniform cross-section, free of impurities. Any nonuniformities (such as ripples) in the final manufactured sheet may be linked back to the fluid dynamics in the molten state. It should therefore prove very useful to study these fluid dynamics in order to see how best to control and optimize the manufacturing process.

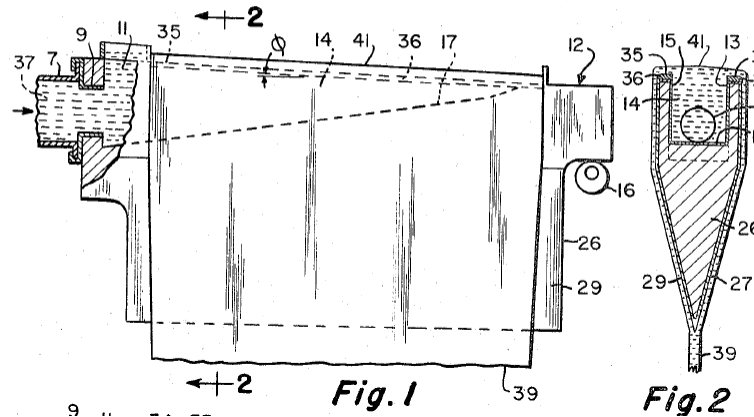


Figure 1: A patent showing the basic design of the overflow glass former apparatus [13].

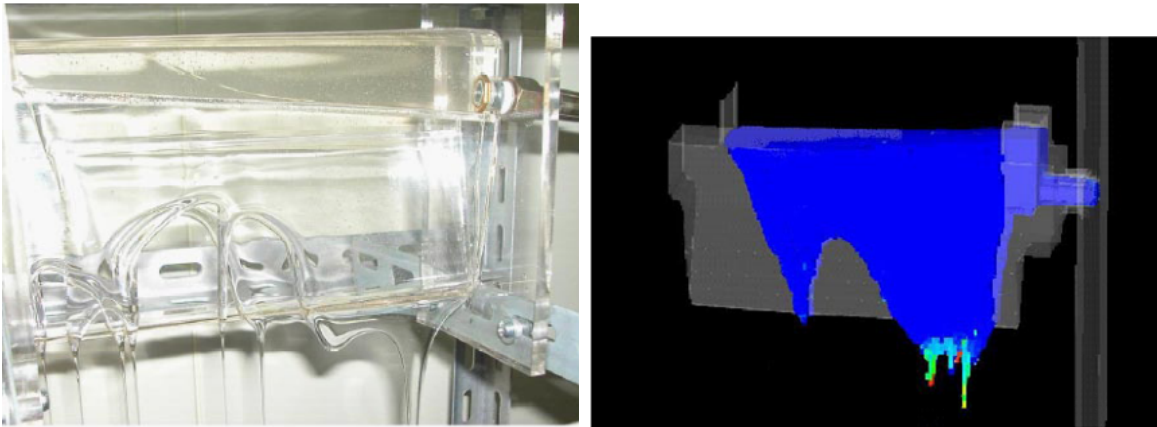


Figure 2: (left) An experiment showing nonuniform dripping in a glass former and (right) computational simulation [12, 22].

Questions of particular interest to Corning include:

- Can we formulate a minimal (asymptotically reduced) yet accurate model for each of the two stages? Corning have some experience with such modeling, but would like to know whether existing models are sufficient, or whether extra physics is needed.
- Thermal gradients in the direction of film flow will obviously be important. But what about the effect of thermal variations across the film thickness? Might these be significant, and can we accurately model them?
- Can we predict what will happen to the leading edge of an advancing front as it travels down the overhang? How will the thermal gradients influence this process?
- What will happen to any impurities present in the original film?

The production process as described above falls naturally into two stages from the fluid-dynamical viewpoint.

Stage 1: The overflow problem In the first stage, molten glass is pumped into the reservoir at a controlled rate. It overflows, and cascades down the exterior walls of the container, which are overhanging inclined planes. See Figs.3 and 4. The flow of the thin layers of molten glass down these

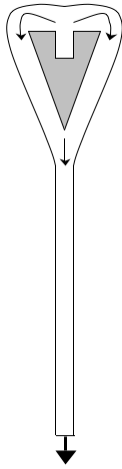


Figure 3: Schematic side-view of sheet former.

inclined planes is modeled using low Reynolds number lubrication theory for viscous fluids. While molten glass may exhibit some viscoelasticity, for simplicity we consider the glass to be a viscous Newtonian fluid, but retain temperature dependence in the viscosity. Our thin film model describes transport due to gravity, surface tension, and Marangoni surface stresses created by temperature gradients along the flow direction. Previous studies without the temperature gradients have shown that instabilities at the leading edge of the advancing sheet (described in the ideal case by a traveling wave solution) can produce fingering (dripping) that is linked to undesirable non-uniformities in the sheet. Our study shows that the temperature gradients modify the flow to have wave-like solutions whose speed changes and whose “capillary-ridge” leading edge structure evolves as the flow advances. Another concern of Corning Inc. is that any tiny impurities such as dust that may settle on the surface of the film as it flows down the incline could be transported along the surface and into the interior of the film by a ‘tank-treading’ motion at the contact line. Our modeling therefore also considers passive scalar transport of possible impurities in the flow.

Stage 2: The falling sheet When the two glass sheets reach the tip of the trough, they will merge together as they fall off in what is called “sheet fusion”, producing a suspended glass sheet in free space. The ideal situation is shown schematically in Figs. 3 and 4. This hanging sheet can be subject to drawing processes to stretch it as it feeds out from the reservoir and cools. The extensional flow model appropriate to this stage of the fluid dynamics reduces to a coupled set of long wave equations for the conservation of the sheet thickness and axial momentum. Further work is needed on this model to integrate it with the outflow from the first stage.

Variants of these two sub-problems have been considered in the past by many authors, working on a variety of different applications, so a range of relevant literature exists. With regard to manufacturing processes in the glass industry, Ellison & Cornejo [14] have recently published a review of glass substrates for liquid crystal displays, in which they describe the history of the device design back to the original Dockerty patent of Fig.1 [13]. Of relevance to problem stage 1 is the large literature on viscous flow down inclined planes. The paper by Troian *et al.* [30] in 1989 reported on the hydrodynamic fingering instability observed at the edge of such an advancing front and has led to extensive further work. Of particular relevance to the set-up here are papers by Lin & Kondic [21] on viscous Newtonian flow down an overhanging plane, and studies of film flows driven by temperature gradients by Cazabat *et al* [11], Bertozzi, Münch *et al* [4–6, 9, 23], and Troian [19].

With regard to stage 2 of the process, again, many references on the evolution of free viscous films exist, incorporating a variety of physical mechanisms. Our approach is in the spirit of work by Howell & co-workers [10, 16] in which systematic asymptotic expansions are used to derive a closed system of PDEs governing the evolution of the sheet’s thickness and axial velocity. We derive a variant of such models, in which the effects of temperature gradients (leading to viscosity gradients and surface tension

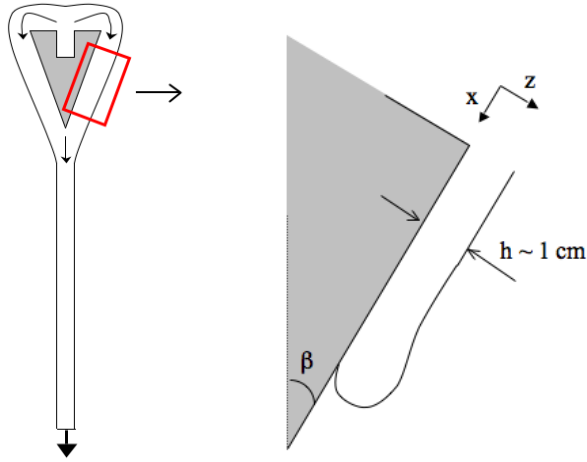


Figure 4: (a) Side-view of the glass-forming apparatus showing the overflow, flow down the inclined walls and fusion yielding a sheet of glass in free-space. (b) Schematic of an enlarged view of the leading edge glass flow (non-wetting case) on the inclined plane with coordinate system shown.

gradients) are also taken into account.

The report structure is outlined below.

- Section 2: Lubrication flow down the sides of the trough, with a view to investigating:
 - Structure and instabilities of the leading edge of the flow (drips and rivulets);
 - ‘Tank treading’ of the contact line and passive transport of impurities;
 - How temperature variations affect stability.
- Section 3: Extensional flow of the fused viscous sheet hanging beneath the trough, with a view to investigating how variations in viscosity both along the sheet and across the sheet affect the fluid flow.
- Conclusions, including assessment of the accuracy of the models used, and possible influence of neglected effects.

2 Lubrication flow problem

In this section we apply lubrication theory to describe the flow of the molten glass along the inverted inclined planes that lie under the reservoir tank. The apparatus is usually designed to be symmetric so that the two thin films are nominally identical and should merge evenly.

While the true rheological properties of glass may be more complicated and might be more fully modeled by some viscoplastic or viscoelastic non-Newtonian constitutive laws [1], we will treat it as a slow, viscous, incompressible Newtonian fluid flow. However we will take into consideration that properties of the fluid (viscosity μ and surface tension γ) may be temperature-dependent, to incorporate effects resulting from the large range of temperatures that will be experienced in the full glass-forming process. The velocity field $\vec{\mathbf{u}}$ and pressure p for the flow will obey the Navier-Stokes equations,

$$\rho \left(\frac{\partial \vec{\mathbf{u}}}{\partial t} + \vec{\mathbf{u}} \cdot \nabla \vec{\mathbf{u}} \right) = -\nabla p + \nabla \cdot (\mu (\nabla \vec{\mathbf{u}} + \nabla^T \vec{\mathbf{u}})) - \rho \vec{\mathbf{g}}, \quad \nabla \cdot \vec{\mathbf{u}} = 0, \quad (1)$$

where the viscosity μ may be spatially dependent (it will be a function of the local glass temperature, which may vary both spatially and temporally). We pick our coordinate system to be aligned with the inclined plane, see Fig. 4, with x being in the direction of flow, y the transverse direction in the plane and z normal to the plane with $(u, v, w) = \vec{\mathbf{u}}$ being the components of the velocity field in those

respective directions. In terms of this coordinate system, the acceleration due to gravity takes the form $\vec{g} = (g \cos \beta, 0, g \sin \beta)$. The complete description of the problem must also include boundary conditions along the entire boundary of the glass flow. At the inclined plane, which we treat as being fixed and impermeable, we will impose no flux and no slip conditions on the velocity field. At the free surface, the geometric definition of the free surface as moving material surface yields the kinetic boundary condition, and we impose a stress balance including influences of the surface tension of the glass and its temperature-dependent variations (the capillary and Marangoni effects respectively).

For low Reynolds number flow as found in this industrial process, we can neglect the inertial terms, yielding the Stokes equations

$$\vec{0} = -\nabla p + \nabla \cdot (\mu(\nabla \vec{u} + \nabla^T \vec{u})) - \rho \vec{g}, \quad \nabla \cdot \vec{u} = 0. \quad (2)$$

Then, for thin glass films, the ratio of the height-scale h_0 to the lengthscales in the plane L yields a small aspect ratio, $\epsilon \equiv h_0/L \ll 1$. In this asymptotic limit (the lubrication limit) the Stokes equations reduce to the system

$$-\rho g \sin \beta = \frac{\partial p}{\partial z}, \quad -\nabla_{\parallel} p + \frac{\partial^2 (\mu \vec{u}_{\parallel})}{\partial z^2} - \rho g \cos \beta \hat{\mathbf{i}} = \vec{0}, \quad \nabla_{\parallel} \cdot \vec{u}_{\parallel} + \frac{\partial w}{\partial z} = 0, \quad (3)$$

where we have separated the velocity and spatial gradient into parts parallel to the solid surface (\vec{u}_{\parallel} and ∇_{\parallel}), and the perpendicular components (w and ∂z): $\vec{u} = \vec{u}_{\parallel} + w \hat{\mathbf{k}}$, where $\vec{u}_{\parallel} = (u, v)$ and $\nabla_{\parallel} \equiv (\partial_x, \partial_y)$. These equations describe the velocity field within the glass film, $0 \leq z \leq h(x, y, t)$ where $z = h(x, y, t)$ is the film's free surface. Starting from (3)₁, we obtain the form of the quasi-static pressure. Treating (3)₂ as an ODE for \vec{u}_{\parallel} in the z -direction and applying the no-slip and stress balance boundary conditions at $z = 0$ and $z = h$ respectively yields the tangential velocity field in terms of the evolving film height and material parameters,

$$\vec{u}_{\parallel} = \frac{z^2 - 2hz}{2\mu} [\rho g \cos \beta \hat{\mathbf{i}} - \rho g \sin \beta \nabla h - \gamma \nabla(\nabla^2 h)] + \frac{\tau z}{\mu} \hat{\mathbf{i}}, \quad (4)$$

where γ is the surface tension and τ is a measure of the Marangoni stress generated by a nonuniform applied temperature, $\tau \equiv d\gamma/dx = \gamma'(\theta)d\theta/dx$. Details of the intermediate steps above have been omitted as these are standard in the literature on thin film flows [26–28], particularly relevant references for flows on inclined planes include [20,21,25], while relevant references including the effects of Marangoni forcing include [5, 6, 11, 23, 24].

The last step of the derivation of the lubrication equation for $h(x, y, t)$ is also standard, but we reproduce it since it will be of help for one of the questions we address later. The kinematic boundary condition at $z = h$ takes the form

$$\frac{\partial h}{\partial t} + \vec{u}_{\parallel} \cdot \nabla_{\parallel} h = w. \quad (5)$$

Integrating equation (3)₃ with respect to z and applying the no-flux boundary condition at $z = 0$ gives

$$w(x, y, z, t) = - \int_0^z \nabla_{\parallel} \cdot \vec{u}_{\parallel} dz'. \quad (6)$$

Substituting the result from (6) for $w(x, y, h(x, y, t), t)$ into (5) yields a statement of conservation of mass in the thin film flow,

$$\frac{\partial h}{\partial t} + \nabla_{\parallel} \cdot \left(\int_0^h \nabla_{\parallel} \cdot \vec{u}_{\parallel} dz' \right) = 0, \quad \left(\text{or equivalently } \frac{\partial h}{\partial t} + \nabla_{\parallel} \cdot \vec{q}_{\parallel} = 0 \right), \quad (7)$$

(the flux \vec{q}_{\parallel} can also be interpreted as in terms of a depth-averaged velocity, $\vec{q}_{\parallel} = h \vec{v}_{\parallel}$). Substituting in (4) yields a single governing PDE for the evolution of the film height,

$$\frac{\partial h}{\partial t} + \frac{\partial}{\partial x} \left(\frac{\tau}{2\mu} h^2 + \frac{\rho g \cos \beta}{3\mu} h^3 \right) = -\nabla \cdot \left(\frac{\rho g \sin \beta}{3\mu} h^3 \nabla h \right) - \nabla \cdot \left(\frac{\gamma}{3\mu} h^3 \nabla(\nabla^2 h) \right) \quad (8)$$

where we will omit the notation indicating the tangent component from here on.

We note that an assumption implicit in deriving the lubrication equation is that h is smooth with slowly varying gradients; this implies a contact line with a small contact angle (low slope), called the wetting case. Lubrication models also have problems with the dynamics of contact lines – namely fluids spreading into previously dry regions. There are several mathematically- or physically-motivated regularizations to this problem, the simplest being the adding of a “prewetting layer” – a very thin pre-existing coating of the fluid everywhere (“complete wetting”); this generally is not expected to change the overall dynamics of the flow for large film thicknesses. Physically, even a monolayer of fluid molecules, can smooth the path of an advancing fluid compared with a completely dry substrate. Mathematically, the degenerate form of the last term in (8) for $h \rightarrow 0$ is problematic in terms of the regularity and uniqueness of solutions with moving contact lines [2]; having a slightly pre-wet surface with a uniform lower bound on the film thickness, $h = b > 0$ avoids such issues.

Before pursuing mathematical analysis of this model, we re-write it in a dimensionless form. We rescale lengths and time according to

$$h = h_0 \tilde{h} \quad x = L \tilde{x} \quad t = \frac{\mu_0 L}{\rho g h_0^2} \tilde{t}$$

where the timescale has been selected based on the speed of gravity-driven viscous flows, and where μ_0 a typical or mean value of the viscosity, which is scaled as

$$\mu = \mu_0 \tilde{\mu}(\tilde{x})$$

to yield the non-dimensionalized equation

$$\frac{\partial h}{\partial t} + \frac{\partial}{\partial x} \left(\frac{\text{Ma}}{2\mu(x)} h^2 + \frac{\cos \beta}{3\mu(x)} h^3 \right) = -\nabla \cdot \left(\frac{D \sin \beta}{3\mu(x)} h^3 \nabla h \right) - \nabla \cdot \left(\frac{\text{Ca}}{3\mu(x)} h^3 \nabla (\nabla^2 h) \right). \quad (9)$$

The other dimensionless parameters are

$$\text{Ma} = \frac{\tau}{\rho g h_0} \quad D = \frac{h_0}{L} \quad \text{Ca} = \frac{\gamma h_0}{\rho g L^3}. \quad (10)$$

Lubrication models are formally derived as leading order equations in perturbation expansions for $\epsilon \equiv h_0/L \rightarrow 0$. In this context, the D term (due to the component of gravity normal to the plane), is a higher order term and should not appear in (9) as the leading order equation. However, for flow down inverted planes, this is a destabilizing term and even if it has a small coefficient, its inclusion has a significant effect and is necessary to fully capture the dynamics of the problem. In the absence of the regularizing capillarity term, the first term on the right-side of (9) would make the model ill-posed, with solutions that would blow-up instantaneously, even with infinitesimally small $D > 0$.

Some previous studies that have used this model include [17, 21], where isothermal problems are considered. In [17] this term is emphasized and the D coefficient is normalized (which selects a lengthscale for L), suggesting a balance between the second- and fourth-order spatial operators. PDE analysis of thin film equations with such balances between destabilizing second-order effects and stabilizing fourth-order surface tension effects, $h_t = -(h^m h_x)_x - (h^n h_{xxx})_x$ [7, 8, 33] suggests that finite-time blow-up of the film thickness (corresponding to the formation and growth of a pendant drop) cannot occur unless the destabilizing term is sufficiently stronger than the fourth-order term, if $m \geq n + 2$. In [17], the differences between the cases of films on inclined and horizontal inverted plates with respect to blow-up are described.

We note that the Ma-term in (9) assumes a constant Marangoni stress, namely there is a uniform gradient of the surface tension in response to the imposed temperature gradient; this tends to drive thin film flows from hot regions to colder ones. A constant stress is consistent with the simplifying assumptions of a linear dependence of the surface tension on temperature and a linear imposed temperature profile. This model has been used in many recent studies of thermal Marangoni effects [5, 6, 11, 23, 24]. In these studies, it was shown that interesting dynamics (undercompressive shocks and partial suppression of fingering instabilities) can occur when the Marangoni stress opposes the gravity-driven flow.

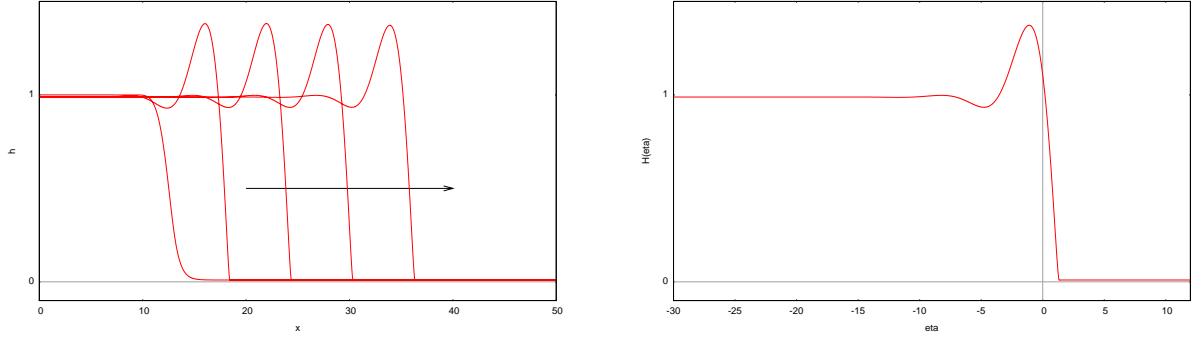


Figure 5: (left) Evolution to the traveling wave solution of (11) in shown in a fixed reference frame, (right) the steady-profile traveling wave solution $H(\eta)$.

2.1 Traveling wave solutions with constant viscosity

In the previous studies of thermal Marangoni driven flows, the temperature-dependence of the viscosity had been treated as a weak effect, and hence ignored. Then the viscosity is treated as a constant and (9) reduces to

$$\frac{\partial h}{\partial t} + \frac{\partial}{\partial x} \left(\frac{\text{Ma}}{2} h^2 + \frac{\cos \beta}{3} h^3 \right) = -\nabla \cdot \left(\frac{D \sin \beta}{3} h^3 \nabla h \right) - \nabla \cdot \left(\frac{\text{Ca}}{3} h^3 \nabla (\nabla^2 h) \right) \quad (11)$$

The structure of advancing uniform contact lines in (11) can be obtained as traveling wave solutions having a steady height profile moving with a constant speed c , $h(x, t) = H(\eta)$ where $\eta = x - ct$. This ansatz reduced (11) to the traveling wave ODE

$$-c \frac{dH}{d\eta} + \frac{d}{d\eta} \left(\frac{\text{Ma}}{2} H^2 + \frac{\cos \beta}{3} H^3 \right) = -\frac{d}{d\eta} \left(\frac{D \sin \beta}{3} H^3 \frac{dH}{d\eta} \right) - \frac{d}{d\eta} \left(\frac{\text{Ca}}{3} H^3 \frac{d^3 H}{d\eta^3} \right). \quad (12)$$

Traveling waves will asymptotically approach constant upstream and downstream heights for $|\eta| \rightarrow \infty$; if the heightscale is normalized with respect to the upstream film thickness, then these are

$$H(\eta \rightarrow -\infty) = 1 \quad H(\eta \rightarrow \infty) = b \ll 1, \quad (13)$$

where b is the thickness of the precursor/prewetting layer. It is straightforward to show that the wavespeed must be given by

$$c = \frac{g(1) - g(b)}{1 - b} \quad g(H) = \frac{\text{Ma}}{2} H^2 + \frac{\cos \beta}{3} H^3. \quad (14)$$

The traveling wave solutions can be obtained using ODE shooting methods, but these can be tricky to implement numerically [31]. An alternative is to write the one-dimensional version of (11) in the moving reference frame for $H(\eta, t)$ and allow for evolution in time to the stable-in-one-dimension steady profile $H(\eta, t) \rightarrow H(\eta)$,

$$\frac{\partial H}{\partial t} - c \frac{\partial H}{\partial \eta} + \frac{\partial}{\partial \eta} \left(\frac{\text{Ma}}{2} H^2 + \frac{\cos \beta}{3} H^3 \right) = -\frac{\partial}{\partial \eta} \left(\frac{D \sin \beta}{3} H^3 \frac{\partial H}{\partial \eta} \right) - \frac{\partial}{\partial \eta} \left(\frac{\text{Ca}}{3} H^3 \frac{\partial^3 H}{\partial \eta^3} \right), \quad (15)$$

starting from generic initial conditions satisfying the boundary conditions, see Fig. 5. Further computations were done to see how the structure of the solution depends on the Marangoni and capillary parameters, see Fig. 6. Since Ca multiplies the highest order derivative in (12), for the limit $\text{Ca} \rightarrow 0$, this equation is a singularly perturbed problem and the capillary ridge can be analyzed as a boundary layer within the framework of matched asymptotics. Its width is expected to scale with $O(\text{Ca}^{1/3})$, and this appears to be borne out, at least qualitatively (see Fig. 6(right)).

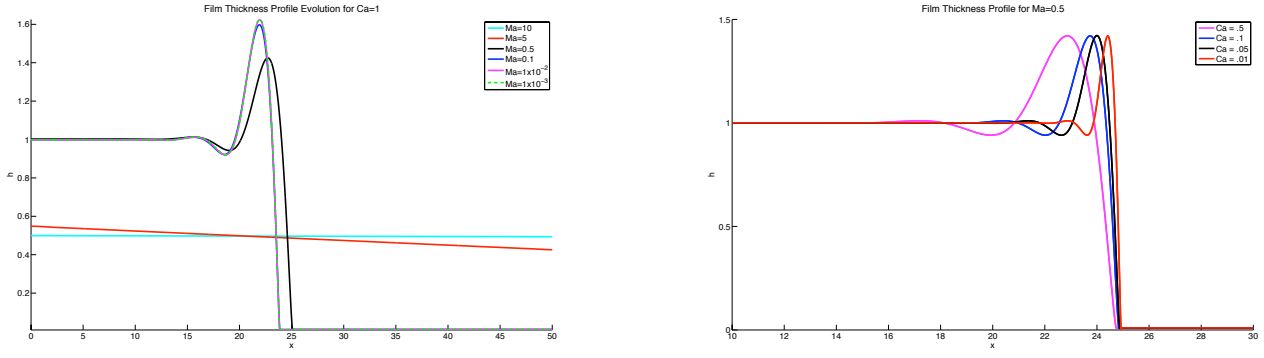


Figure 6: (left) Varying the Marangoni number Ma , (right) Varying the capillary number Ca .

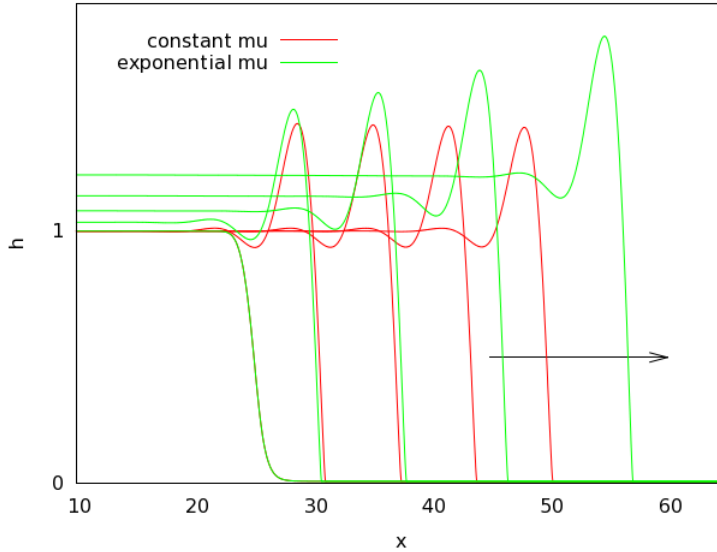


Figure 7: Comparison of traveling wave solutions for fixed viscosity vs. slowly evolving solutions with viscosity controlled by a fixed temperature profile, $\mu(x) = e^{x/200}$.

2.2 Temperature dependent viscosity

Traveling wave solutions to (11) are possible because the equation is translationally invariant. If the dependence of the viscosity on temperature is retained, as in (9) with a fixed imposed temperature field, then the equation has non-autonomous coefficients and is no longer translation-invariant. However, solutions have a similar structure, though their amplitude and speed may exhibit slow variations over time. Fig. 7 shows a solution of (9) alongside the analogous solution of (11). Both solutions have the same initial condition, and the same values for the system parameters: $Ca = 1$, $Ma = 1/2$, $D = 1/5$, $\beta = 20^\circ$ and are shown at the same times. The red curves (solutions of (11)) show the expected traveling wave behavior, but for the green curves (solutions of (9)), the dimensionless viscosity is prescribed by $\mu(x) = e^{x/200}$, modeling the effect of a decreasing temperature profile along the substrate, as x increases. The simple exponential model was chosen for computational convenience and its results were somewhat counter-intuitive and sparked further group discussions. It might be expected that flow into a region with increasing viscosity would have a decreasing characteristic speed, however the figure shows a front with a steadily increasing speed. One possible competing influence is that the gradient in the viscosity creates an additional flux of fluid (note the rising upstream film thickness) which might accelerate the front despite the retarding influence of the spatially increasing viscosity; further study should be given to this point.

2.3 A coupled model including heat transfer

A more realistic model would allow for an evolving temperature field controlled by heat transfer at the substrate and heat flow through the evolving thin film [18]. Consequently, “ $\mu(x)$ ” in (9) would be replaced by $\mu(\theta(x, t))$ where θ is the effective temperature and $\text{Ma} \rightarrow \widetilde{\text{Ma}} \partial_x \theta$. We suppose that the temperature is determined by the convective heat equation, and that heat is lost through the substrate by conduction, and into the air by radiation. The model for the temperature θ reads

$$\rho c_p (\theta_t + u\theta_x + w\theta_z) = k (\theta_{xx} + \theta_{zz}), \quad (16)$$

$$\theta_z = \alpha (\theta - \theta_s) \quad \text{on} \quad z = 0, \quad (17)$$

$$\frac{-\theta_z + h_x \theta_x}{\sqrt{1 + h_x^2}} = \beta (\theta^4 - \theta_a^4) \quad \text{on} \quad z = h. \quad (18)$$

Here, c_p is the specific heat capacity of the fluid, k is the thermal conductivity, α and β are transfer coefficients, and θ_s and θ_a are the (assumed uniform and constant) temperatures in the substrate and air respectively.

Under the assumption that the Peclet number, $\text{Pe} = \rho^2 g L c_p h_0^2 / (\bar{\mu} k) \sim O(1)$ and the transfer coefficients $\alpha^* = \alpha L^2 / (k h_0)$ and $\beta^* = \beta \theta_a^3 L^2 / (k h_0) \sim O(1)$, we find that the leading-order solution¹ to (16-18) is $\theta = \theta(x, t)$. We use the equations and boundary conditions at next order to obtain a preliminary (nondimensional) model for the evolution of the temperature field:

$$\text{Pe} h (\theta_t + \bar{u} \theta_x) = (h \theta_x)_x - \beta^* (\theta^4 - 1) - \alpha^* (\theta - \theta^*). \quad (19)$$

where $\theta^* = \theta_s / \theta_a$, and the temperature has been scaled with the air temperature. This distinguished limit (and its sub-limits) hold providing that $\text{Pe} h_0^2 / L^2$, $\alpha h_0 / k$, $\beta \theta_a^3 h_0 / k \ll 1$. If the transfer coefficients are larger, we can obtain solutions which vary across the film (*e.g.*, if $\alpha h_0 / L$, $\beta \theta_a^3 h_0 / L \gg 1$, we find that $\theta = \theta^* (1 - z/h) + z/h$).

The final modelling step is to couple the surface tension and the temperature. The simplest relationship is to say that the surface tension decreases linearly as the temperature increases, *i.e.*

$$\gamma(\theta) = \gamma_0 - \lambda \theta. \quad (20)$$

2.4 Two-dimensional stability analysis

An important further step in the analysis of the flow is the study of the stability of the uniform flow to perturbations in the transverse direction. Transverse perturbations can lead to fingering instabilities and growing perturbations, that corrupt the desired uniformity of sheets and coatings.

If we ignore the spatial variation of the viscosity, *i.e.* set $\mu(x) \equiv 1$ in (9) to regain (11), we can consider infinitesimal perturbations to the uniform film $h = 1$ far behind the contact line in the form $h \approx 1 + \delta e^{i(\ell x + k y) + \sigma t}$ with $\delta \ll 1$. Substituting into (11) and retaining linear terms, we obtain the dispersion relation:

$$\sigma = -i\ell(\text{Ma} + \cos \beta) + (\ell^2 + k^2) \left(D \sin \beta - \frac{\text{Ca}}{3} (\ell^2 + k^2) \right). \quad (21)$$

The imaginary part of this relation connects to convection due to the Marangoni stress and tangential component of gravity; this determines a phase speed of $c_{ph} = \text{Ma} + \cos \beta$ for infinitesimal waves. The real part of the dispersion relation shows that the system is long-wave unstable; perturbations with wavelengths greater than $\lambda_c = 2\pi \sqrt{\text{Ca} / [3D \sin \beta]}$ are expected to grow in amplitude and the modes with maximum growth rate $\lambda_* = 2\pi \sqrt{2\text{Ca} / [3D \sin \beta]}$ are expected to dominate based on linear theory. The Marangoni parameter does not enter into this critical wavelength, but may be important

¹Here we formally use $\theta = \theta_0 + \epsilon^2 \theta_1 + \dots$, where $\epsilon = h_0 / L$ and present the solution for θ_0 .

in distinguishing between convective and absolute instabilities. More thorough study of rivulets and fingering instabilities requires analysis of transverse perturbations to the traveling wave profile,

$$h(x, y, t) \approx H(x - ct) + \delta g(x - ct) \cos(ky) e^{\sigma t} \quad \delta \ll 1. \quad (22)$$

This stability analysis, which must be written in terms of operators involving derivatives of $H(\eta)$, must, for the most part, be carried out numerically [3, 15], since the leading-order traveling wave about which we perturb is not available in closed form, but only numerically.

2.5 Particle trajectories

One question of particular interest for these flows is how impurities are transported in the flow. Based on the no-slip boundary condition at the substrate, impurities on the substrate should remain fixed in place. Impurities that deposit onto the free-surface of the film will move with the flow and will exhibit a 'tank-tread' rolling near the contact line [32].

To illustrate ideas for particle pathlines in lubrication flows, we first consider the canonical problem of flow in a two-dimensional spreading drop. The porous medium equation,

$$h_t = D(h^3 h_x)_x \quad (23)$$

describes spreading of viscous drops on a horizontal plate due to gravity. This is a special case of the main equation with $\text{Ma} = \text{Ca} = 0$, $\beta = \pi/2$ and $D \rightarrow -D$. The component of the velocity along the plate is given by

$$u = \frac{Dh_x}{2}(z^2 - 2hz) \quad (24)$$

then from (6) the normal component of the velocity is

$$w = \frac{D}{2} \left(\frac{1}{2}(h^2)_{xx} z^2 - \frac{1}{3} z^3 \right) \quad (25)$$

Equation (23) has a closed-form explicit similarity solution describing infinite-time spreading of finite-mass initial conditions. Seeking a similarity solution in the form $h = t^\alpha f(x/t^\beta)$ yields

$$h(x, t) = t^{-1/5} \left[K - \frac{3x^2}{10D t^{2/5}} \right]_+^{1/3}, \quad (26)$$

for a droplet symmetric about $x = 0$, where K is a constant of integration depending on the initial condition. Substituting (26) into (24, 25) yields the ODE system for particle pathlines:

$$\frac{dx}{dt} = u(x, z, t) \quad \frac{dz}{dt} = w(x, z, t) \quad \text{for } 0 \leq z(t) \leq h(x(t), t) \quad (27)$$

The solutions of this system are plotted in Fig. 8.

A similar procedure may be carried out for the traveling-wave solution of (12) (the case in which the dependence of the viscosity on temperature is assumed weak, so that traveling waves exist). By substituting a numerical representation of the traveling wave solution $H(\eta)$ of (12) into (4, 6) we can numerically compute the corresponding particle paths, using equations (27). Some representative particle paths are shown in Fig. 9. As with our previous numerical simulations, we alleviate the stress singularity at the moving contact line with a thin precursor film ahead of the moving front. We observe that fluid particles sitting very close to the free interface near the moving front are readily transported to the fluid's interior. This suggests that small dust particles or other impurities present during manufacture could, if they land on the film, be transported inside the glass sheet, leading to permanent defects.

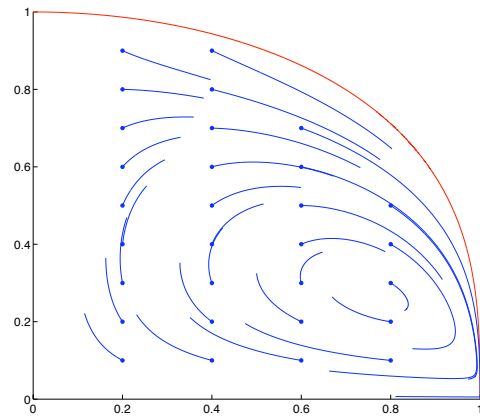


Figure 8: Particle paths in a spreading viscous drop in the porous medium equation.

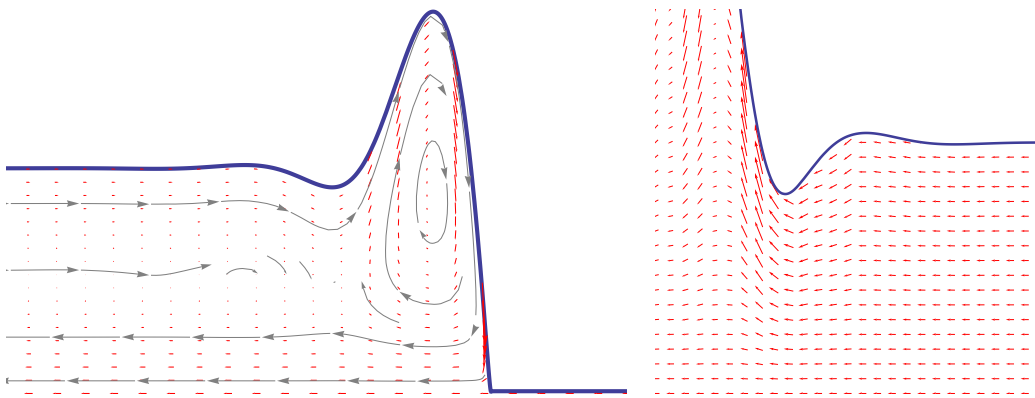


Figure 9: (left) Particle paths in the advancing contact line flow (right) detail of the flow field at the base of the capillary ridge.

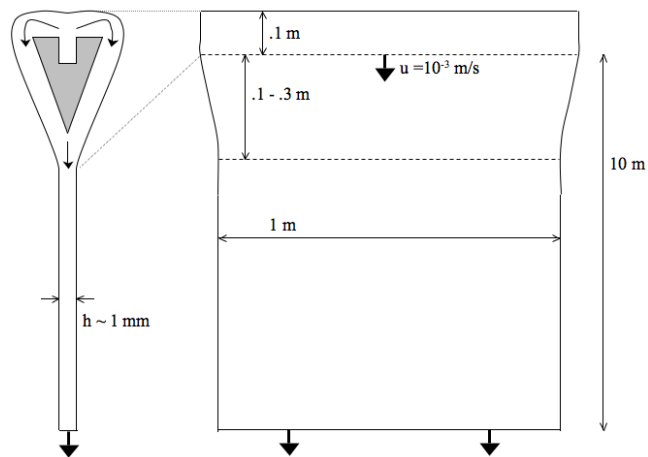


Figure 10: The hanging sheet geometry, with approximate dimensions.

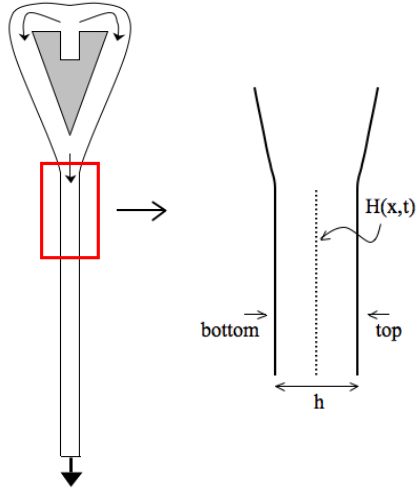


Figure 11: Model for extensional flow: schematic of the region of interest.

3 Extensional flow

3.1 Modeling

In this section we consider the second part of the manufacturing process, in which the two advancing fronts on the two outer sides of the trough have merged (“fused”) underneath the trough, and fall down under gravity (and possibly externally-applied forces also) as a single sheet in extensional flow. Our approach closely follows that of Howell [16], though we include the effects of the temperature-dependent viscosity, which was absent from that work.

The relevant forces here are gravity and surface tension, and since temperature θ varies, both surface tension and viscosity, which are functions of temperature, will vary along/throughout the sheet. As in the work of Howell [16] we assume a nearly-planar sheet, such that the ratios of typical thickness, h_0 , and centerline deviation, H_0 , to a typical sheet length L , are both small: $h_0/L, H_0/L \sim \epsilon \ll 1$.

Scaling the transverse coordinate, sheet thickness and centerline deviations with h_0 , we define the dimensionless sheet centerline, $z = H(x, t)$, and its thickness $h(x, t)$, so that its free surfaces are defined by $z = H \pm h/2$.

With gravity in the x -direction, and a reduced pressure \bar{p} scaled with $\mu_0 U/L$ (where μ_0 is a typical viscosity and U a typical axial velocity), our dimensionless governing equations (correct to order ϵ^2) are

$$-\epsilon^2 \bar{p}_x + (\mu u_z)_z + 2\epsilon^2 (\mu u_x)_x + \epsilon^2 (\mu w_x)_z = 0, \quad (28)$$

$$-\bar{p}_z + 2(\mu w_z)_z + (\mu u_z)_x + \epsilon^2 (\mu w_x)_x = 0, \quad (29)$$

$$u_x + w_z = 0, \quad (30)$$

subject to a kinematic boundary condition, and normal and tangential stress balances at the two free surfaces,

$$\left. \begin{aligned} w &= (H \pm h/2)_t + u(H \pm h/2)_x \\ \mathbf{n} \cdot \boldsymbol{\sigma} \cdot \mathbf{n} &= \gamma^\pm \kappa, \\ \mathbf{t} \cdot \boldsymbol{\sigma} \cdot \mathbf{n} &= \gamma_s^\pm, \end{aligned} \right\} \text{on } z = H \pm h/2.$$

To obtain a closed system of equations governing the evolution of the sheet, we first expand the dependent variables \bar{p} , u , w in powers of ϵ^2 . At leading order, we find extensional flow $u_0(x, t)$ (in the obvious notation for the leading-order longitudinal velocity), but the problem is not closed. We need to expand both the Navier-Stokes equations (in the form given above) and the boundary conditions to order ϵ^2

to obtain a closed system of PDEs for the leading-order quantities u_0 , h_0 , H_0 . We also assume that the surface tension γ can be decomposed as $\gamma^\pm = \gamma_0 + (\Delta\gamma)\gamma_{1x}^\pm(x, t)$, where γ_0 is constant, and $\Delta\gamma/\gamma_0$ is $O(\epsilon^2)$ (see [10]). The procedure is similar to that outlined in [10] (though complicated here by the variable viscosity), hence we do not give the details of this calculation. Dropping the zero superscript on any leading-order quantities for simplicity, the result is the following three equations:

$$\begin{aligned} 4(h\bar{\mu}u_x)_x + St h + \frac{1}{2Ca} h h_{xxx} + Ma(\gamma_{1x}^+ + \gamma_{1x}^-) &= 0, \\ h_t + (uh)_x &= 0, \\ H_{xx} &= 0, \end{aligned}$$

where the dimensionless Stokes, capillary and Marangoni numbers are defined by $St = \rho g L^2 / (\mu_0 U)$, $Ca = \mu_0 U / (\epsilon \gamma_0)$, $Ma = \Delta\gamma / (\epsilon \mu_0 U)$, and were all assumed to be $O(1)^2$ in the derivation.

Here, $\bar{\mu}(x, t)$ is a cross-sheet averaged viscosity defined by

$$\bar{\mu} = \frac{1}{h} \int_{H-h/2}^{H+h/2} \mu dz, \quad (31)$$

and γ_{1x}^\pm are surface tension gradients on the two free surfaces.

We can immediately see that a variation of the viscosity across the sheet does not cause it to bend, and that the only the average value of the viscosity matters in determining the film thickness and glass velocity. We note that corrections to the velocity, thickness and centreline are at $O(\epsilon^2)$, indicating that the thin-film approximation should accurately predict the evolution of the sheet generated by CFD studies initiated by Corning.

In the simplest of cases, where we set $St, Ma = 0$ and $Ca = \infty$, the steady state solution, assuming that we know h at the top of the film, and the flux Q and tension T at the bottom of the film, is

$$h = h_0 \exp \left[-\frac{T}{4Q} \int_0^x \frac{dx}{\bar{\mu}} \right] = h_0 \exp \left[\frac{Tk}{4Q} (e^{-x/k} - 1) \right] \quad (32)$$

when $\bar{\mu} = e^{x/k}$. In particular, at the bottom of the sheet, the thickness becomes

$$h = h_0 \exp \left[-\frac{Tk}{4Q} \right], \quad (33)$$

and we can see straight away that increasing the viscosity (i.e. decreasing k) can keep h close to h_0 .

Incorporating the capillary term would involve a calculation following that presented for a foam lamellae in [10].

We note that the centreline of the sheet will bend if there is a pressure difference from one side to the other, and in this case the centreline equation becomes:

$$H_{xx} = \frac{Ca}{2} (P^+ - P^-), \quad (34)$$

with P^\pm the pressures either side of the sheet. If these external pressures are constant, they neither alter the film thickness nor the velocity.

Of course, as in the previous section, we should track the temperature field in the film, write the viscosity and surface tensions as functions of temperature, and solve the four coupled equations together. This is a difficult problem, which we are keen to pursue outside the study group forum.

²These choices give a distinguished limit of the problem. Another distinguished limit has the Marangoni and capillary terms balancing at leading order, and a parabolic velocity profile across the sheet

3.2 Bending stiffness

A viscous fluid sheet can suffer both stretching and bending effects and these effects can be coupled depending upon the orientation of the sheet, its thickness, viscosity and lateral extent. In the modelling process we have ignored the effect the bending stiffness and which can add an extra level of complexity to the analysis. To at least partially justify this omission we estimate the bending stress associated with the fluid and a solid with an appropriate set of parameters. For a solid the effective stiffness of the material is characterized by the Young's modulus and for a fluid it is the viscosity with respect to the time scale for the flowing of the sheet that is the important parameter.

First assuming that the glass sheet is a solid with a Young's modulus E , the cross-sheet characteristic bending stress is given by

$$B_{\text{solid}} = \frac{1}{hL} \int_{-h/2}^{h/2} z \sigma_{xx} dz, \quad (35)$$

where the stress component $\sigma_{xx} = -\kappa E z$ with $\kappa = \partial^2 w / \partial x^2$ the the corresponding curvature. Scaling the curvature as h/L^2 gives a characteristic size for the bending stress of

$$[B_{\text{solid}}] \sim \frac{1}{hL} \frac{E h^3}{12} \frac{h}{L^2} = \frac{E}{12} \epsilon^3. \quad (36)$$

In a similar fashion, the corresponding bending stress for a thin viscous sheet is given by [29]

$$[B_{\text{fluid}}] \sim \frac{\mu U}{3L} \epsilon^2. \quad (37)$$

To answer whether or not bending stiffness should be included we consider a typical set of parameters $U \sim 3 \times 10^{-3} \text{ ms}^{-1}$, $L = 1 \text{ m}$, $h = 10^{-3} \text{ m}$, $\mu = 6800 \text{ Pa}\cdot\text{s}$, $E \sim 10^7 \text{ Pa}$ and we find that $[B_{\text{solid}}] \sim 10^{-3}$ and $[B_{\text{fluid}}] \sim 10^{-5}$.

It is clear from this that the fluid bending stress can be thought of as a secondary effect because of the slow speed of the slab. At this speed, the fluid bending moment only plays a role at very high ($\epsilon EL/4U \sim 10^6 \text{ Pa}\cdot\text{s}$) viscosities. Below these viscosities the sheet can be treated as solid with respect to the bending stiffness.

4 Conclusion

In section 2 we formulated lubrication models for the flow of the molten glass along the inclined tank walls. If (as assumed) the glass cools as it flows down the incline then Marangoni surface stresses ($\text{Ma} > 0$) augment the influence of effect of gravity in driving the flow and instabilities of advancing contact lines are expected [3]. If the temperature gradient is in the opposite direction, undercompressive shocks can occur, which change the structure and stability properties of the advancing contact line. In particular, this changes how disturbances ahead/behind the front propagate [9] and would have an influence on the pathlines for impurities carried in the flow, i.e. § 2.5. Previous studies of thin film flows with thermal Marangoni effects have generally neglected accompanying variations in the viscosity (since those variations were relatively small). In the current problem, since the temperature variation is expected to be substantial these effects may have a stronger role and should be studied further.

In section 3 we considered the evolution of the falling glass sheet. We derived an extensional flow model for determining the thickness and centreline of the sheet and the (extensional) velocity of the glass. Our model immediately showed that the presence of a nonuniform viscosity was not able to bend the sheet, but that the evolution would be affected.

Of course, we should invest effort in establishing a model in which the transition from lubrication flow to extensional flow is considered, in order to fully explain the behaviour of this method of glass manufacture.

References

- [1] N. J. Balmforth, R. V. Craster, A. C. Rust, and R. Sassi. Viscoplastic flow over an inclined surface. *Journal of Non-Newtonian Fluid Mechanics*, 142:219–243, 2007.
- [2] A. L. Bertozzi. The mathematics of moving contact lines in thin liquid films. *Notices Amer. Math. Soc.*, 45(6):689–697, 1998.
- [3] A. L. Bertozzi and M. P. Brenner. Linear stability and transient growth in driven contact lines. *Phys. Fluids*, 9(3):530–539, 1997.
- [4] A. L. Bertozzi, A. Münch, X. Fanton, and A. M. Cazabat. Contact line stability and ”undercompressive shocks” in driven thin film flow. *Phys. Rev. Lett.*, 81(23):5169–5172, 1998.
- [5] A. L. Bertozzi, A. Münch, and M. Shearer. Undercompressive shocks in thin film flows. *Phys. D*, 134(4):431–464, 1999.
- [6] A. L. Bertozzi, A. Münch, M. Shearer, and K. Zumbrun. Stability of compressive and undercompressive thin film travelling waves. *European J. Appl. Math.*, 12(3):253–291, 2001. The dynamics of thin fluid films.
- [7] A. L. Bertozzi and M. C. Pugh. Long-wave instabilities and saturation in thin film equations. *Comm. Pure Appl. Math.*, 51(6):625–661, 1998.
- [8] A. L. Bertozzi and M. C. Pugh. Finite-time blow-up of solutions of some long-wave unstable thin film equations. *Indiana Univ. Math. J.*, 49(4):1323–1366, 2000.
- [9] M. Bowen, J. Sur, A. L. Bertozzi, and R. P. Behringer. Nonlinear dynamics of two-dimensional undercompressive shocks. *Physica D*, 209:36–48, 2005.
- [10] C. J. W. Beward and P. D. Howell. The drainage of a foam lamella. *J. Fluid Mech.*, 458:275–298, 2002.
- [11] A. M. Cazabat, F. Heslot, S. M. Troian, and P. Carles. Finger instability of thin spreading films driven by temperature gradients. *Nature*, 346(6287):824–826, August 1990.
- [12] W.-K. Chang. Experiment and simulation of overflow fusion process for flat glass. Master’s thesis, National United University, Taiwan, 2006. http://ethesys.nuu.edu.tw/ETD-db/ETD-search/view_etd?URN=etd-0725106-212727.
- [13] S. M. Dockerty. Sheet forming apparatus. *United States Patent Office*, 3,338,696, 1967.
- [14] A. Ellison and I. A. Cornejo. Glass substrates for liquid crystal displays. *International Journal of Applied Glass Science*, 1(1):88–103, 2010.
- [15] A. A. Golovin, B. Y. Rubinstein, and L. M. Pismen. Effect of van der waals interaction on the fingering instability of thermally driven thin wetting films. *Langmuir*, 17:3930–3936, 2001.
- [16] P. D. Howell. Models for thin viscous sheets. *European J. Appl. Math.*, 7(4):321–343, 1996.
- [17] A. Indeikina, I. Veretennikov, and H.-C. Chang. Drop fall-off from pendent rivulets. *Journal of Fluid Mechanics*, 338:173–201, 1997.
- [18] O. E. Jensen and J. B. Grotberg. The spreading of heat or soluble surfactant along a thin liquid film. *Physics of Fluids A*, 5(1):58–68, 1993.
- [19] D. E. Kataoka and S. M. Troian. A theoretical study of instabilities at the advancing front of thermally driven coating films. *J. Colloid and Interface Science*, 192:450–362, 1997.

- [20] L. Kondic. Instabilities in gravity driven flow of thin fluid films. *SIAM Rev.*, 45(1):95–115 (electronic), 2003.
- [21] L. Kondic and T.-S. Lin. Thin films flowing down inverted substrates: Two dimensional flow. *Physics of Fluids*, 22:052105, 2010.
- [22] H.-J. Lin and W.-K. Chang. Design of a sheet forming apparatus for overflow fusion process by numerical simulation. *Journal of non-crystalline solids*, 353:2817–2825, 2007.
- [23] A. Münch. Shock transitions in Marangoni gravity-driven thin-film flow. *Nonlinearity*, 13(3):731–746, 2000.
- [24] A. Münch and A. L. Bertozzi. Rarefaction—undercompressive fronts in driven films. *Phys. Fluids*, 11(10):2812–2814, 1999.
- [25] A. Münch and B. A. Wagner. Numerical and asymptotic results on the linear stability of a thin film spreading down a slope of small inclination. *European J. Appl. Math.*, 10(3):297–318, 1999.
- [26] T. G. Myers. Thin films with high surface tension. *SIAM Rev.*, 40(3):441–462, 1998.
- [27] J. R. Ockendon and H. Ockendon. *Viscous flow*. Cambridge University, Cambridge, 1995.
- [28] A. Oron, S. H. Davis, and S. G. Bankoff. Long-scale evolution of thin liquid films. *Reviews of Modern Physics*, 69(3):931–980, 1997.
- [29] N. M. Ribe. Bending and stretching of thin viscous sheets. *Journal of Fluid Mechanics*, 433:135–160, 2001.
- [30] S. A. Safran S. M. Troian, E. Herbolzheimer and J. F. Joanny. Fingering instabilities of driven spreading films. *Europhys. Lett.*, 10(1):25–30, 1989.
- [31] E. O. Tuck and L. W. Schwartz. A numerical and asymptotic study of some third-order ordinary differential equations relevant to draining and coating flows. *SIAM Rev.*, 32(3):453–469, 1990.
- [32] E. B. Dussan V. and S. H. Davis. On the motion of a fluid-fluid interface along a solid surface. *Journal of Fluid Mechanics*, 65:71–95, 1974.
- [33] T. P. Witelski, A. J. Bernoff, and A. L. Bertozzi. Blowup and dissipation in a critical-case unstable thin film equation. *European J. Appl. Math.*, 15(2):223–256, 2004.